Electronic Supplementary Material (ESI) for ChemComm.

Supporting Information for

N- and O-Doped Mesoporous Carbons Derived from Rice Grains: Efficient Metal-free Electrocatalysts for Hydrazine Oxidation

Katherine Koh,[§a] Yuying Meng,[§b] Xiaoxi Huang,[a] Xiaoxin Zou,[c] Manish Chhowalla[d] and Tewodros Asefa[*ae]

[a] Department of Chemistry and Chemical Biology, Rutgers, The State University of New Jersey, Piscataway, New Jersey 08854, United States.

[b] School of Chemistry, Sun Yat-Sen University, Guangzhou 510275, P. R. China.

[c] State Key Laboratory of Inorganic Synthesis and Preparative Chemistry, International Joint Research Laboratory of Nano-Micro Architecture Chemistry, College of Chemistry, Jilin University, Changchun 130012, P. R. China.

[d] Department of Materials Science and Engineering, Rutgers, The State University of New Jersey, Piscataway, New Jersey 08854, United States.

[e] Department of Chemical and Biochemical Engineering, Rutgers, The State University of New Jersey, Piscataway, New Jersey 08854, United States.

Corresponding Author: tasefa@rci.rutgers.edu

Author Contributions: [§] These authors contributed equally.

1. Details of Experimental Procedures

1.1. Materials and Reagents

Colloidal silica dispersion (Ludox® HS-40, 40 wt. % suspension in water, particle size ≈ 12 nm), hydrazine monohydrate, phosphate buffer saline solution (PBS, 1X, pH = 7.4), and Pt/C (20 wt. %) were purchased from Sigma-Aldrich. Sodium hydroxide (NaOH) and absolute ethanol were obtained from Fisher Scientific. Raw rice was acquired from Seoul Trading Kyung-Gi rice (Product of 2014, Milled rice, purchased in USA). The rice grains have particles *ca.* 6 mm width and *ca.* 2 mm diameter. Elemental analysis indicated that the rice grains have 40 % of carbon, 7 % of hydrogen, 1.0 % of nitrogen and 52 % oxygen. All the chemicals and materials were used as received without any further purification. Deionized water was used throughout the experiments.

1.2. Instrumentations and Characterizations

The nitrogen adsorption and desorption isotherms of the materials were measured with a Micromeritics TriStar-3000 (Micromeritics Instrument Corp.) at the liquid-nitrogen temperature. In order to remove any possible guest species adsorbed on the samples' surfaces, the samples were first degassed under nitrogen gas at 60 °C for 12 h before the measurements. From the adsorption/desorption data, the Brunauer-Emmett-Teller (BET) surface area and Barrett-Joyner-Halenda (BJH) pore size distribution of the samples were determined. Transmission electron microscope (TEM) images of the as-synthesized materials were acquired with a Topcon 002B TEM instrument. The FT-Raman spectra were acquired using a Raman spectrometer (Renishaw 1000) equipped with a 20 mW air-cooled argon ion laser (λ = 514.5 nm), which served as the excitation lights source. The laser power at the sample position was typically 400 μW and had an average spot-size of 1 μm in diameter. X-ray photoelectron spectra were obtained using a Thermo Scientific K-Alpha X-ray photoemission spectrometer (XPS) equipped with an Al Kα as its X-ray source (hυ =1486.6 eV), with an energy resolution of 0.6 eV for the survey scans and 0.1 eV for high resolution scans of individual peaks. Elemental analyses of the samples were performed at Robertson Microlit Laboratories, Ledgewood, NJ, USA.

1.3. Synthesis of RDMC Materials and Catalysts

1.3.1. Hydrothermal treatment of rice grains (Step 1)

The first HTC synthetic step (*Step 1*) was carried out in a 25 mL Teflon-lined stainless steel autoclave, which was placed in an oven and subjected to hydrothermal treatment. In a typical experiment, milled raw rice grains (Kyung-gi rice, purchased in USA) (1 g) were mixed with distilled water (10 mL) in a Teflon-lined stainless steel autoclave and then hydrothermally treated at 180 °C for 6 h (*Part 1 of Step 1)*). *Caution!* Autoclaves under hydrothermal conditions should be handled with extreme care, and proper safety protocols have to be followed handling them all the time, especially more so in cases where the volume is less than half of the reactor's volume as in our case here. After letting the mixture cool down to room temperature, different amounts of colloidal silica (0, 0.5, 1, or 2 g per 1 g of rice grain) were added into the mixture. The mixtures were well dispersed under sonication for 30 min, and then subjected to a second hydrothermal treatment at the same temperature (180 °C) for another 6 h (*Part 2 of Step 1*). The autoclave was let to cool down to room temperature. The solid products in the mixture were recovered by centrifugation, washed with distilled water and kept in oven at 100 °C for 12 h to let the solvent in them evaporate. This finally resulted in dark-brown, carbon/colloidal silica composite powder materials.

1.3.2. High temperature pyrolysis (Step 2)

In *Step 2,* the carbon/silica composite materials obtained above were all pyrolyzed at 800 °C in a temperature-programmable tube furnace under a flow of argon at a flow rate of ~30 mL/min. In the experiment, first the furnace temperature was raised to 300 °C with a ramp of 1 °C/min, and kept at this temperature for 3 h. The temperature was then increased to a final, desired temperature of 800 °C at a ramp of 10 °C/min, and kept at this temperature for another 2 h. Finally, the furnace was let to cool down to room temperature, producing different graphitized carbon/silica composite materials.

To study the effect of pyrolysis temperature, another set of materials were prepared from the carbon/colloidal silica composite powder material prepared above with 1 g colloidal silica per 1 g of rice grain. This carbon/silica composite material was pyrolyzed at four different high temperatures (600, 700, 800, or 900 °C) in a temperature-programmable tube furnace under a flow of argon at a flow rate of ~30 mL/min. First the furnace temperature was raised to 300 °C with a ramp of 1 °C/min, and kept at this temperature for 3 h. The temperature was then increased to a final, desired temperature of 600, 700, 800, or 900 °C at a ramp of 10 °C/min, and kept at this temperature for another 2 h. Finally, the furnace was let to cool down to room temperature, producing different graphitized carbon/silica composite materials.

1.3.3. Removal of colloidal silica (step 3)

To remove the silica templates from the graphitized carbon/colloidal silica products, typically 40 mg of the material was mixed with 1 M NaOH solution (20 mL) in autoclave and kept at 100 °C for 18 h. The dispersions were then centrifuged, and the resulting solid products were washed, first with distilled water and then with absolute ethanol (3 x 20 mL in each case). Finally, the obtained materials were dried in oven at 60 °C for 12 h. This led to black as-obtained rice-derived mesoporous carbon materials, which were denoted as RDMC-*T*-*x*, where *T* and *x* represent the final pyrolysis temperature and the amount of colloidal silica per 1 g of rice grains used to make each material.

1.3.4. Synthesis of control materials

For comparison, two control materials were synthesized. The first one was obtained by applying the two consecutive hydrothermal steps, followed by removal of the colloidal silica. The resulting material was denoted as RDC-HTC-1. The second material was prepared by applying only the pyrolysis step on a dried mixture of rice/SiO_2 (1:1 wt. ratio) (*step 2*) before proceeding to step 3. The product was denoted as RDMC-800-Py-1.

1.4. Electrochemical Tests and Electrocatalysis

1.4.1. Preparation of electrodes

The electrochemical and eletrocatalytic properties of all the mesoporous carbon and corresponding control materials were examined with a Versastat3 potentiostat (Princeton Applied Research, PAR). For the tests, a three-electrode cell, which consisted of a saturated calomel electrode (SCE) as the reference electrode, a graphitic carbon rod (diameter: 6 mm) as the counter electrode, and a glassy carbon disk (diameter: 3 mm) containing the catalysts as the working electrode, was used.

For the preparation the working electrode, 2 mg of catalyst was first dispersed in 200 μL of 2-propanol under sonication to form a homogeneous suspension of the catalyst. Then, 2 μL of the resulting suspension was pipetted and drop-casted onto the surface of a freshly polished glassy carbon electrode (GCE) (with diameter of 3 mm). The final loading of catalyst was 283 μg/cm^2. After letting the catalyst-coated GCE dry under ambient conditions, a diluted solution of Nafion (10 %) (2 μL) was casted on it. The electrode was let to dry in air and then became ready for use.

To investigate the possible effect of the Nafion coating on the electrocatalytic activity of the materials, a second working electrode was prepared by placing 2 μL of more concentrated (20 %) Nafion on top of RDMC-800-1-casted glassy carbon electrode. When dried, this gave a thicker coating of Nafion around RDMC-800-1 than the corresponding one prepared using 2 μL of 10 % Nafion.

The working electrode for Pt/C (20 wt. %), which we have used for comparative studies, was prepared in the same way as above. Typically, 2 mg of Pt/C catalyst was first dispersed in 200 μL of 2-propanol under sonication to form a homogeneous suspension of the catalyst. Then, 2 μL of the resulting suspension was pipetted and drop-casted onto the surface of a freshly polished glassy carbon electrode (GCE) (with diameter of 3 mm). The final loading of Pt/C and Pt loading were 283 μg/cm2 and 56.6 μg/cm2, respectively. After letting the catalyst-coated GCE dry under ambient conditions, a diluted solution of Nafion (10 %) (2 μL) was casted on it. The electrode was let to dry in air and then became ready for use. This information has now been included in SI section of the paper.

1.4.2. Cyclic Voltammetry

Cyclic voltammetry (CV) curves during electrocatalysis over the materials synthesized above were performed in a phosphate buffered saline (PBS) solution (0.1 M, pH 7.4). In the CV measurements, the potential was scanned from -0.6 to 0.6 V *vs.* SCE with different scan rates, ranging from 10 to 100 mV/s, and the hydrazine concentration was varied from 10 to 100 mM. All the electrochemical measurements were carried out at room temperature and under ambient pressure.

1.4.3. Rotating disc electrode (RDE)

Linear sweep voltammograms (LSVs) over RDMC-800-1 were acquired with a Pine Bi-potentiostat (Pine Research Instrumentation), using a rotating disc electrode (RDE) (Pine Research Instrumentation). For the experiments, a three-electrode configuration comprising a catalyst-modified glassy carbon as a working electrode was employed. The LSVs were scanned from -0.6 to 0.6 V at a scan rate of 10 mV/s and with the RDE rotating at 900 rpm.

1.4.4. Stability Tests of the Electrocatalysts

The stability of the mesoporous carbon materials during electrocatalysis of HOR was investigated by cyclic voltammetry in 50 mM hydrazine/0.1 M PBS solution. Typically, 500 cycles of LCVs were recorded, and the peak current densities for 50, 100, 150, 200, 250, 300, 350, 400, 450, and 500 cycles were obtained. Additionally, chronoamperometric measurement over the electrocatalysts was performed at a potential of -0.06 V (vs. SCE) in 50 mM hydrazine/0.1 M PBS solution.

2. Additional Results and Discussions

To investigate the effect of the HTC temperature on the structure of the materials, we performed additional experiments by synthesizing three (control) materials using different HTC temperatures: 90, 120, and 150 °C (Table 1). The materials were then all pyrolyzed at 800 °C, and their colloidal silica templates were removed with an alkaline solution. Note that, except for the HTC temperatures used in *Step 1*, the procedures employed to synthesize all the materials were otherwise the same as those used to synthesize RDMC-800-1 (*i.e.*, the material that was made with the HTC temperature of 180 °C and discussed in the paper).

The resulting materials were characterized by TEM and N_2 porosimetry, and their catalytic activities toward hydrazine oxidation reaction were then investigated. The results are complied Table S1 and Figures S3, S4 and S18. Both TEM and N_2 porosimetry show that all the RDMC-800-1 materials prepared with different HTC temperatures have nanoporous structures. The results further show that, although the materials made using lower HTC temperatures have higher surface areas than the one made with HTC temperature of 150 °C (HTC-180 or the RDMC-800-1 discussed in the manuscript), their catalytic activities are still lower that that of the latter. In other words, RDMC-800-1 prepared with HTC-180 still gives the best catalytic activity, or the lowest overpotential and highest peak current density, among all the materials.

To investigate the possible effect of HTC reaction time on the materials' properties, we performed one more control experiment, by varying the first HTC treatment time. Note that, except for the HTC temperature used in *Step 1*, all experimental procedures were otherwise followed in the same way as those used make RDMC-800-1 (which was made with the HTC temperature of 180 °C). The resulting material was characterized, and its electrocatalytic properties were also investigated (see Figures 5 and 6, below). The results are compiled in Figure S5 and Table S2. Note that all experimental procedures were otherwise followed in the same way those used to make RDMC-800-1 (made with the HTC temperature of 180 °C), except the HTC temperatures used in *Step 1*. The results show that the first part of the HTC treatment step doesn't affect BET surface areas of the material; however, RDMC-800-1 with 6 h still shows higher electrocatalytic activity toward HOR than RDMC-800-6.

3. Supporting Results and Figures

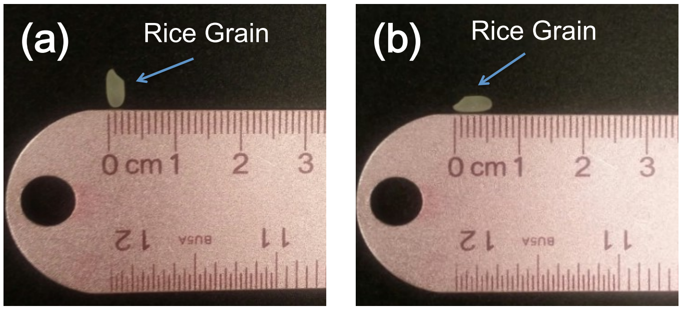

Figure S1. Picture of a rice grain and its size: a) width/diameter and b) length.

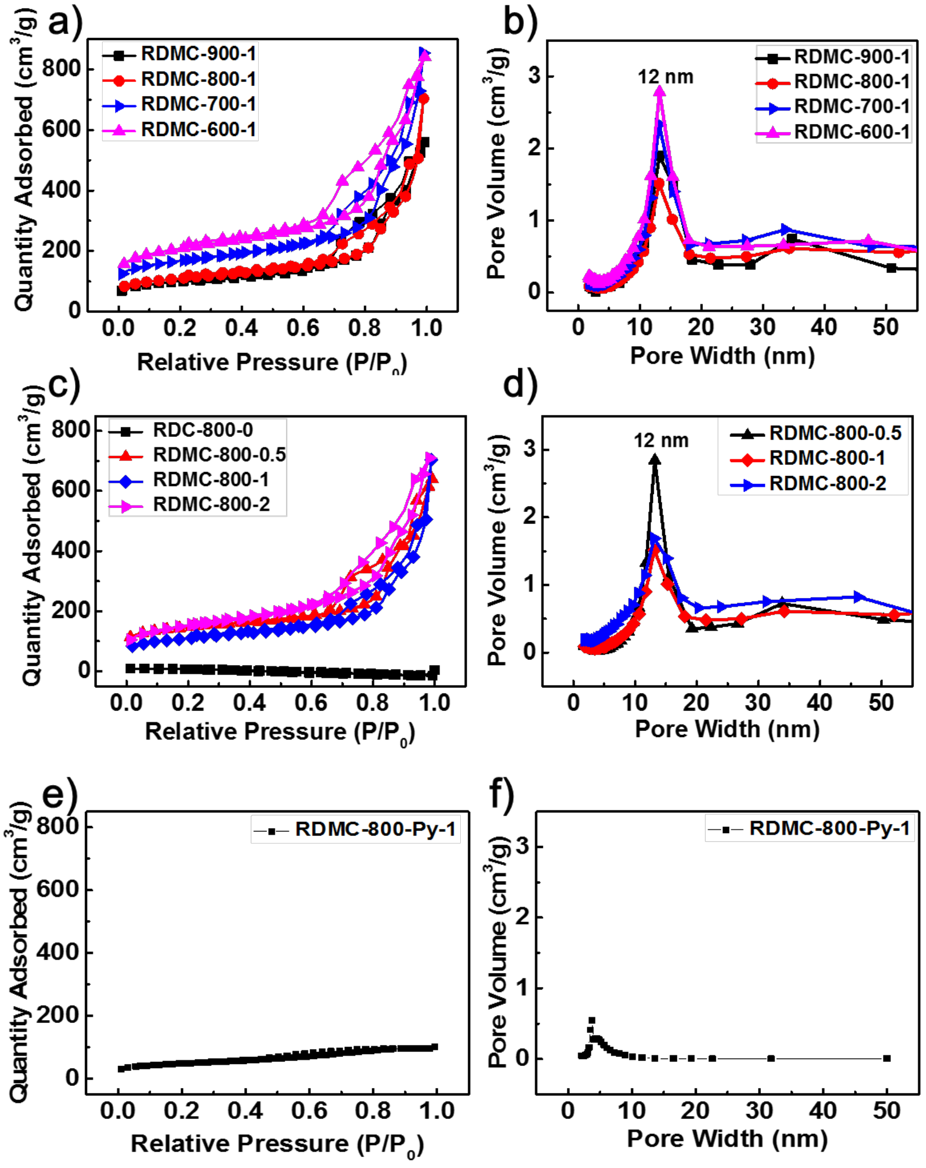

Figure S2. (Left panel) N_2 adsorption/desorption isotherms and (right panel) BJH pore size distributions of: (a,b) the series of RDMC-*T*-1 materials (where *T* is 600, 700, 800, or 900 ºC), (c,d) the series of RDMC-800-*x* (where *x* is the amount of colloidal silica (in g) per 1 g of milled rice grains, and (e-f) the control material RDMC-800-Py-1.

Table S1. Synthetic parameters, including HTC temperature and reaction time, employed to make the various (control) RDMC materials and results of their surface area

RDMC-800-1 Materials Synthesized with Different HTC Temperatures	*Step 1 (HTC Treatments)*[a]		*BET Surface Area* (m^2/g)[b]
	Part 1	*Part 2*	
HTC-90	90 °C, 6 h	90 °C, 6 h	604
HTC-120	120 °C, 6 h	120 °C, 6 h	602
HTC-150	150 °C, 6 h	150 °C, 6 h	357
HTC-180[c]	180 °C, 6 h	180 °C, 6 h	366

[a] In the first part (*Part 1*) of *Step 1*, the HTC treatment did not involve colloidal silica, and in the second part (*Part 2*) of *Step 1*, the HTC treatment was performed in the presence of 1 g of colloidal silica. This step (*Step 1*) was followed by pyrolysis at 800 °C (*Step 2*). [b] Measured by N_2 porosimetry. [c] Same sample as the RDMC-800-1 mentioned in the manuscript.

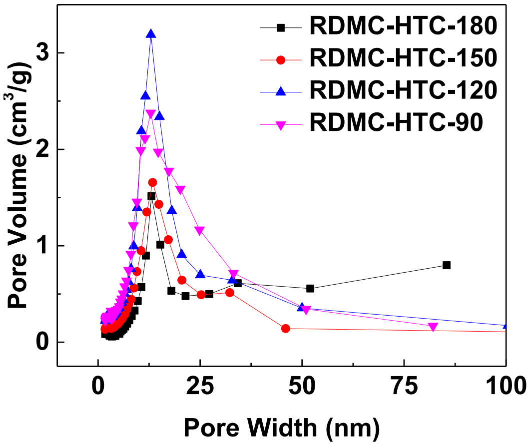

Figure S3. Pore size distribution of control RDMC-800-1 materials prepared by varying the HTC temperature (HTC-90, HTC-120, HTC-150 and HTC-180).

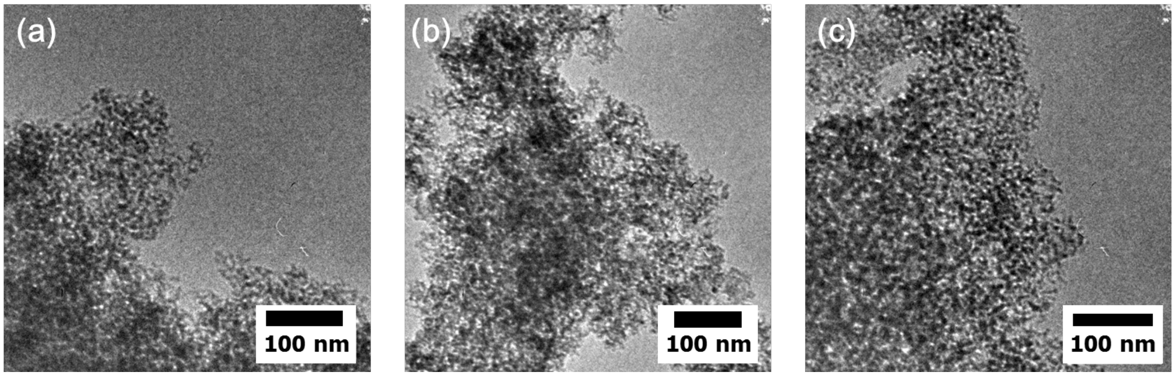

Figure S4. TEM images of the control RDMC-800-1 materials synthesized using different HTC temperatures: a) HTC-90, b) HTC-120, and c) HTC-150.

Table S2. Control samples synthesized by varying HTC reaction time and their surface area[a]

RDMC-800-1 Synthesized with	*Step 1 (HTC Treatments)*		*BET Surface Area (m^2/g)* [b]
	Part 1	*Part 2*	
One HTC step	None	180 °C, 6 h	386
Two HTC steps[c]	180 °C, 6 h	180 °C, 6 h	366

[a] In the synthesis of all the materials, 1 g of colloidal silica was used in the second part of *Step 1*. This was followed by pyrolysis at 800 °C in *Step 2*. [b] Measured by N_2 porosimetry; [c] Same sample with RDMC-800-1 in manuscript

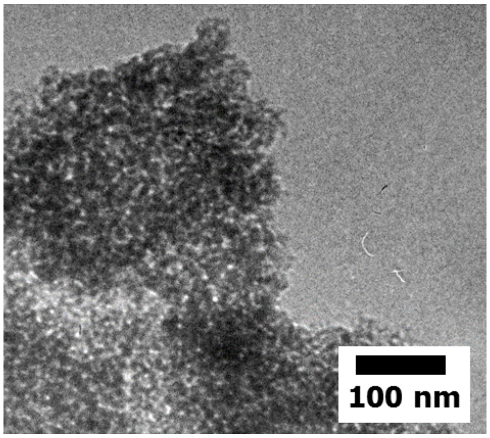

Figure S5. TEM image of RDMC-800-1 material prepared with one HTC treatment step (only for 6 h). Note that the image for the one prepared with two HTC steps (6 h + 6 h HTC treatment) had been included in the paper.

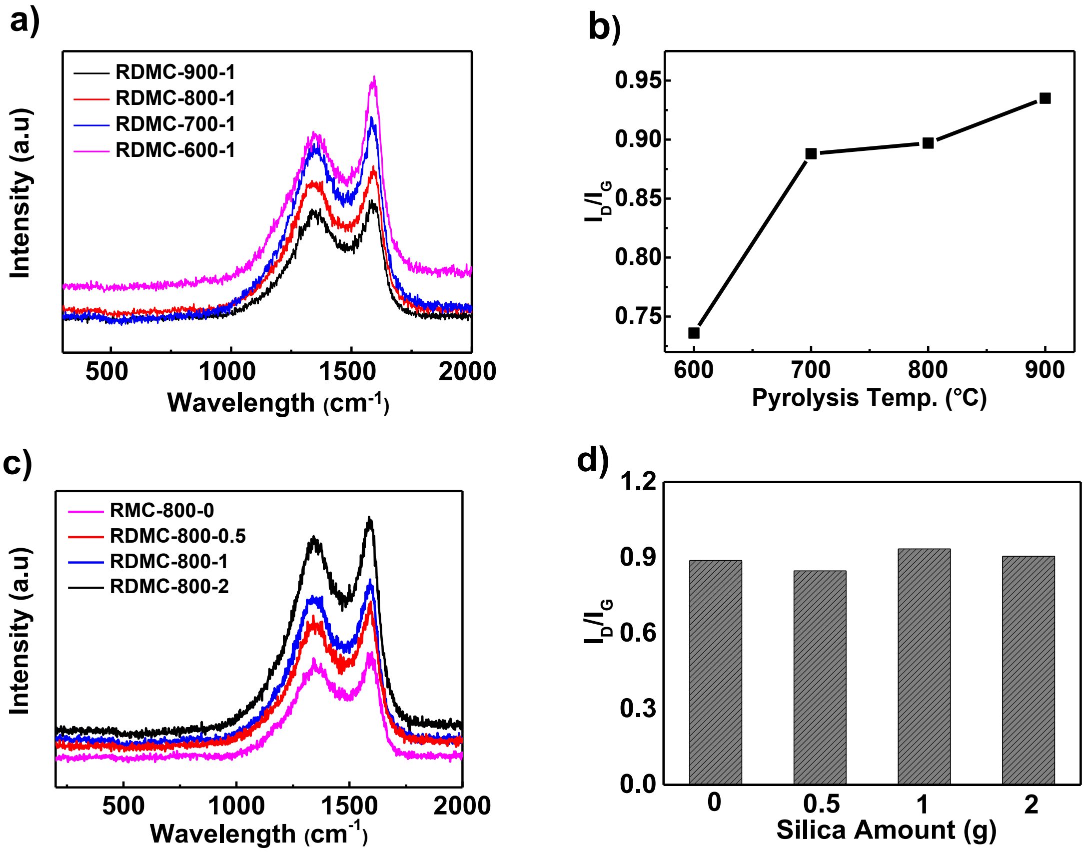

Figure S6. Raman spectra (left panel) and I_D/I_G ratios (right panel) of the RDMC materials obtained under different synthetic conditions: (a-b) the series of RDMC-*T*-1 materials and (c-d) RDMC-800-*x* materials.

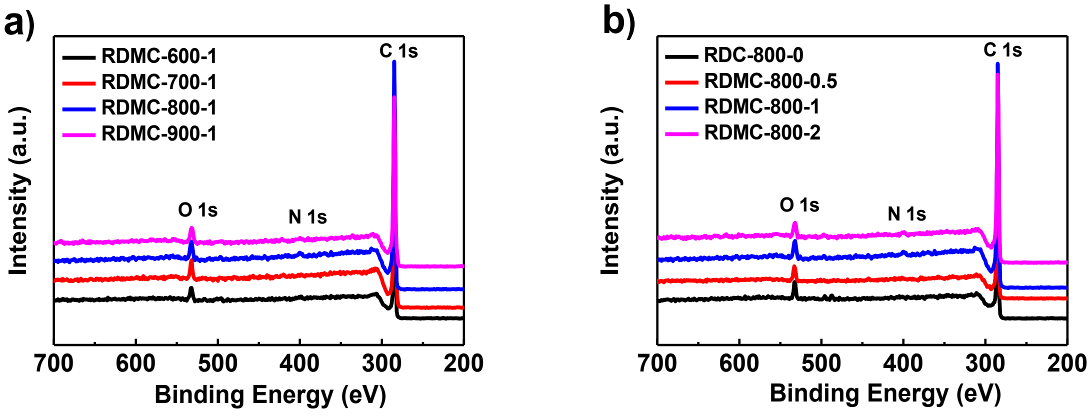

Figure S7. XPS survey spectra of the series of (a) RDMC-*T*-1 and (b) RDMC-800-*x* materials.

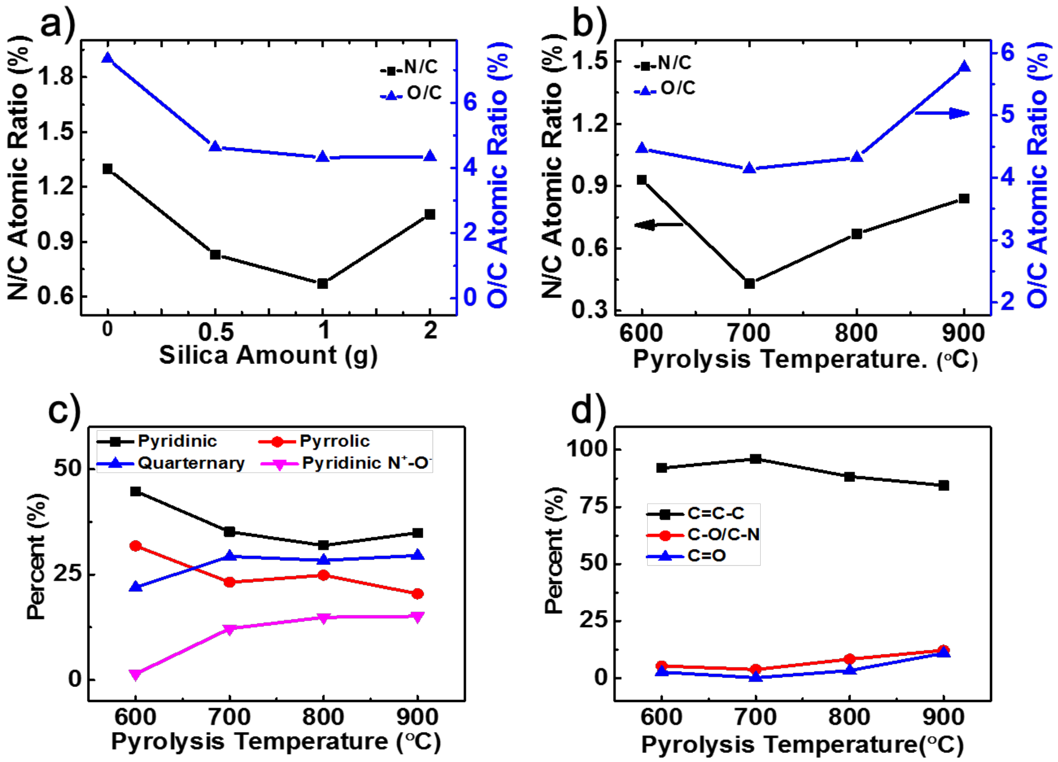

Figure S8. XPS results for RDMC-*T*-*x* materials. a) The N/C and O/C atomic ratios of the series of RDMC-800-*x* materials, b) the N/C and O/C atomic ratios of the series of RDMC-*T*-1 materials, and c) the percentages of the different types of N species and d) atomic percentages of the different C species in the series of RDMC-*T*-1 materials.

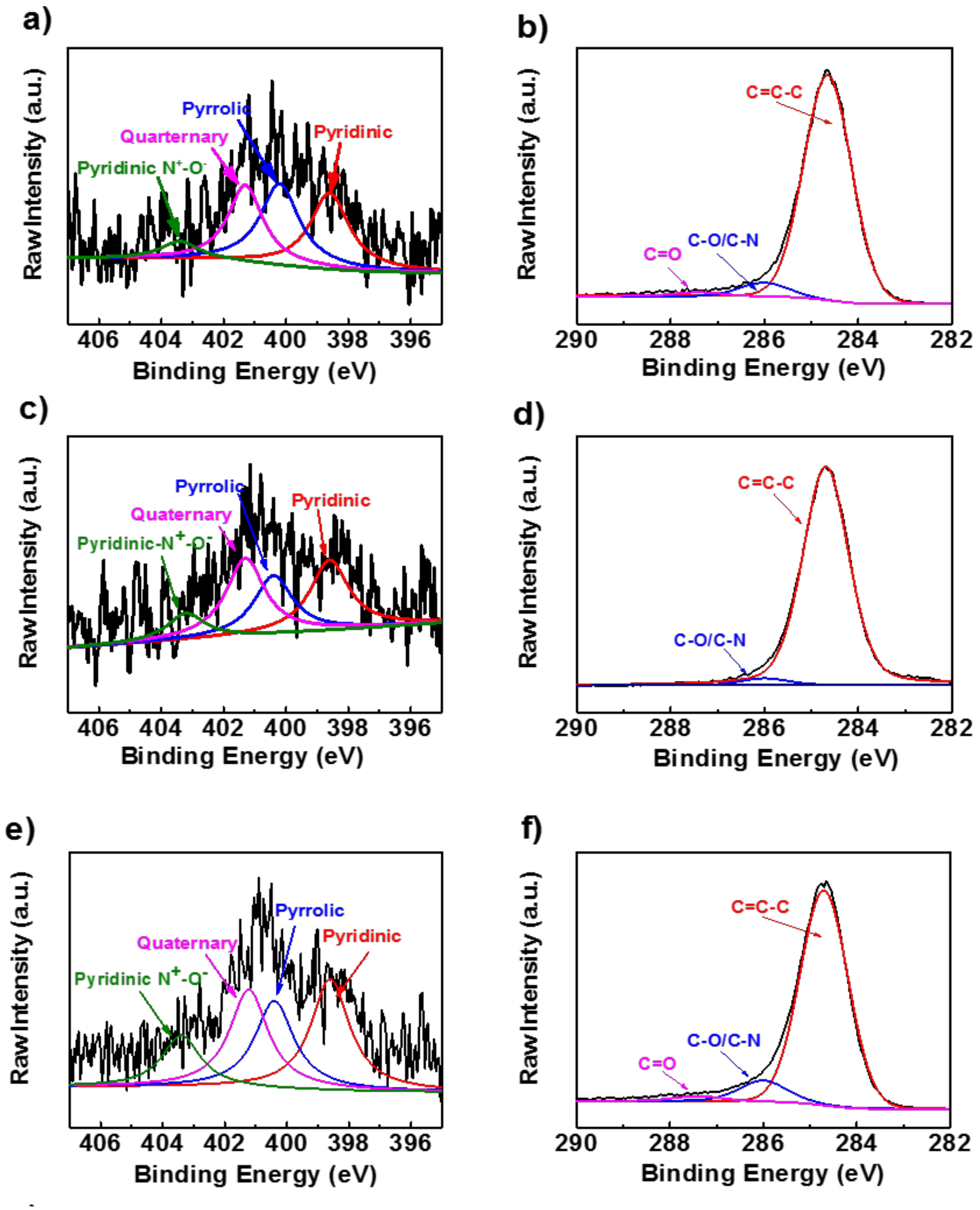
a)
Raw Intensity (a.u.)
Pyrrolic
Quarternary
Pyridinic
Pyridinic N+-O-
406 404 402 400 398 396
Binding Energy (eV)
b)
Raw Intensity (a.u.)
C=C-C
C=O
C-O/C-N
290 288 286 284 282
Binding Energy (eV)
c)
Raw Intensity (a.u.)
Pyrrolic
Quaternary
Pyridinic
Pyridinic-N+-O-
406 404 402 400 398 396
Binding Energy (eV)
d)
Raw Intensity (a.u.)
C=C-C
C-O/C-N
290 288 286 284 282
Binding Energy (eV)
e)
Raw Intensity (a.u.)
Pyrrolic
Quaternary
Pyridinic
Pyridinic N+-O-
406 404 402 400 398 396
Binding Energy (eV)
f)
Raw Intensity (a.u.)
C=C-C
C-O/C-N
C=O
290 288 286 284 282
Binding Energy (eV)

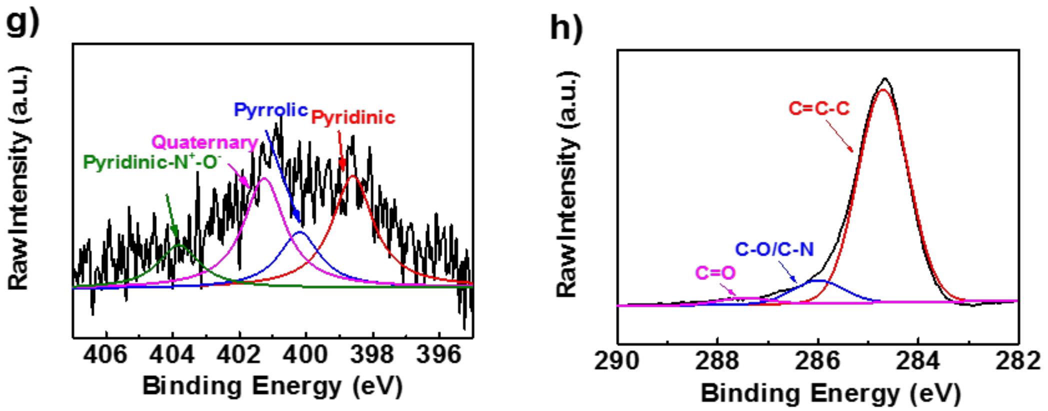

Figure S9. High-resolution XPS spectra of N1s peak (left panels) and C1s peak (right panels) of the series of RDMC-*T*-1 materials, which are synthesized at different pyrolysis temperatures: (a,b) RDMC-600-1, (c,d) RDMC-700-1, (e,f) RDMC-800-1, and (g,h) RDMC-900-1.

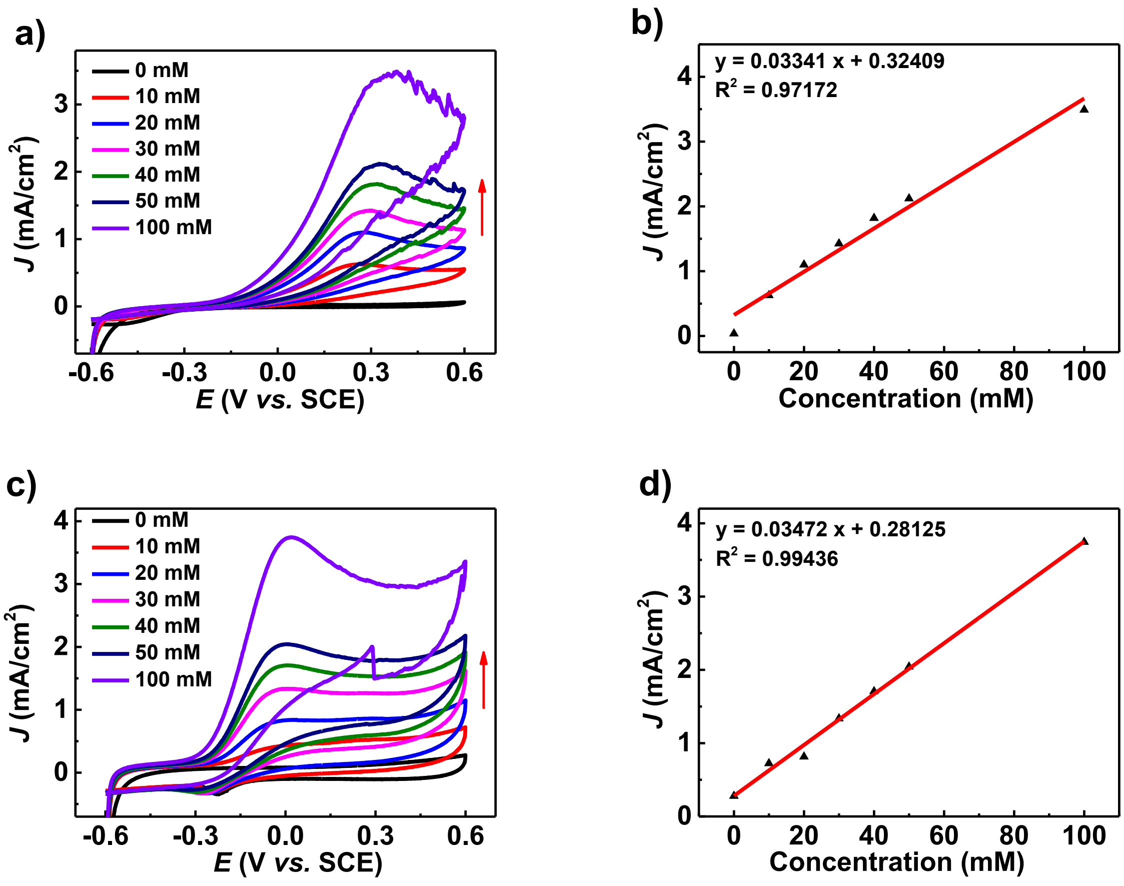

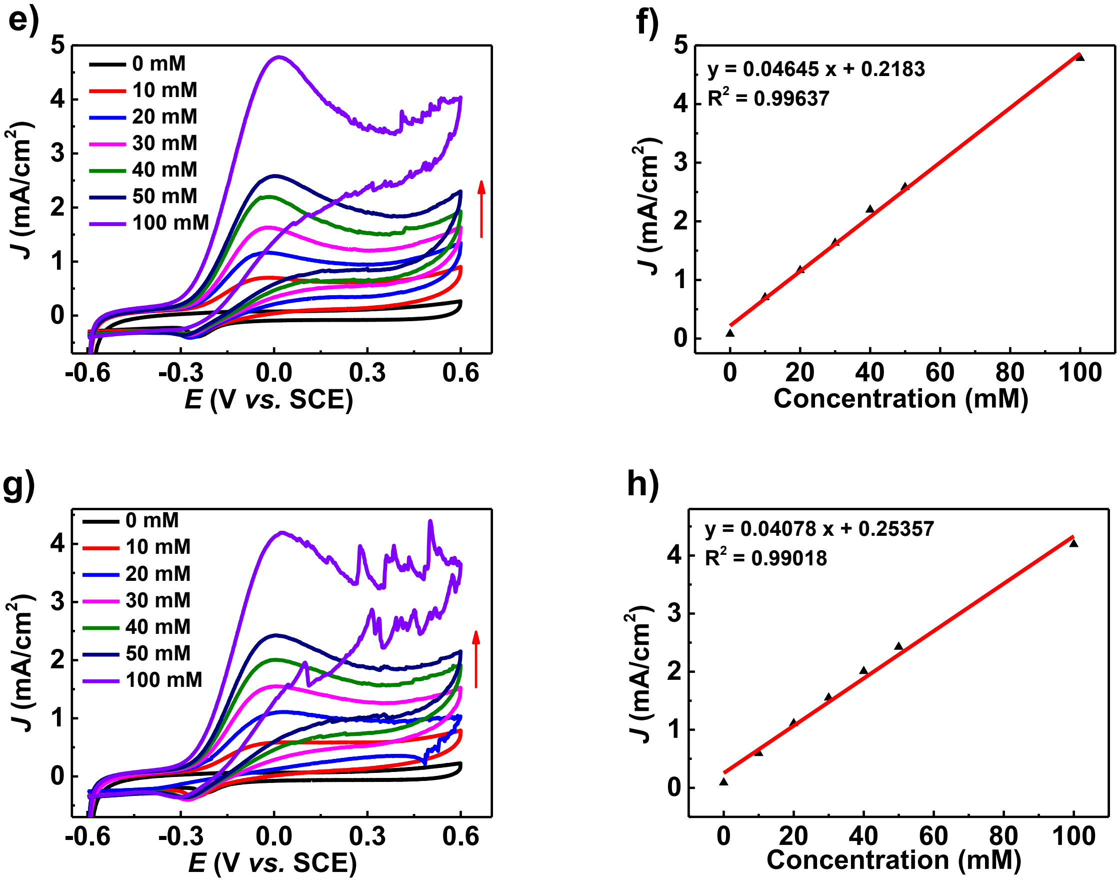

Figure S10. Cyclic voltammograms (CVs) of various concentrations hydrazine electrochemical oxidation with a scan rate of 10 mV/s at pH 7.4 in 0.1 M PBS over different RDMC-800-*x* materials/electrocatalysts (left panels) and their corresponding peaks current density versus hydrazine concentration graphs (right panels). The CVs are for: (a) RDC-800-0, (c) RDMC-800-0.5, (e) RDMC-800-1, and (g) RDMC-800-2. The corresponding current density versus concentration graphs are shown for: (b) RDC-800-0, (d) RDMC-800-0.5, (f) RDMC-800-1 and (h) RDMC-800-2.

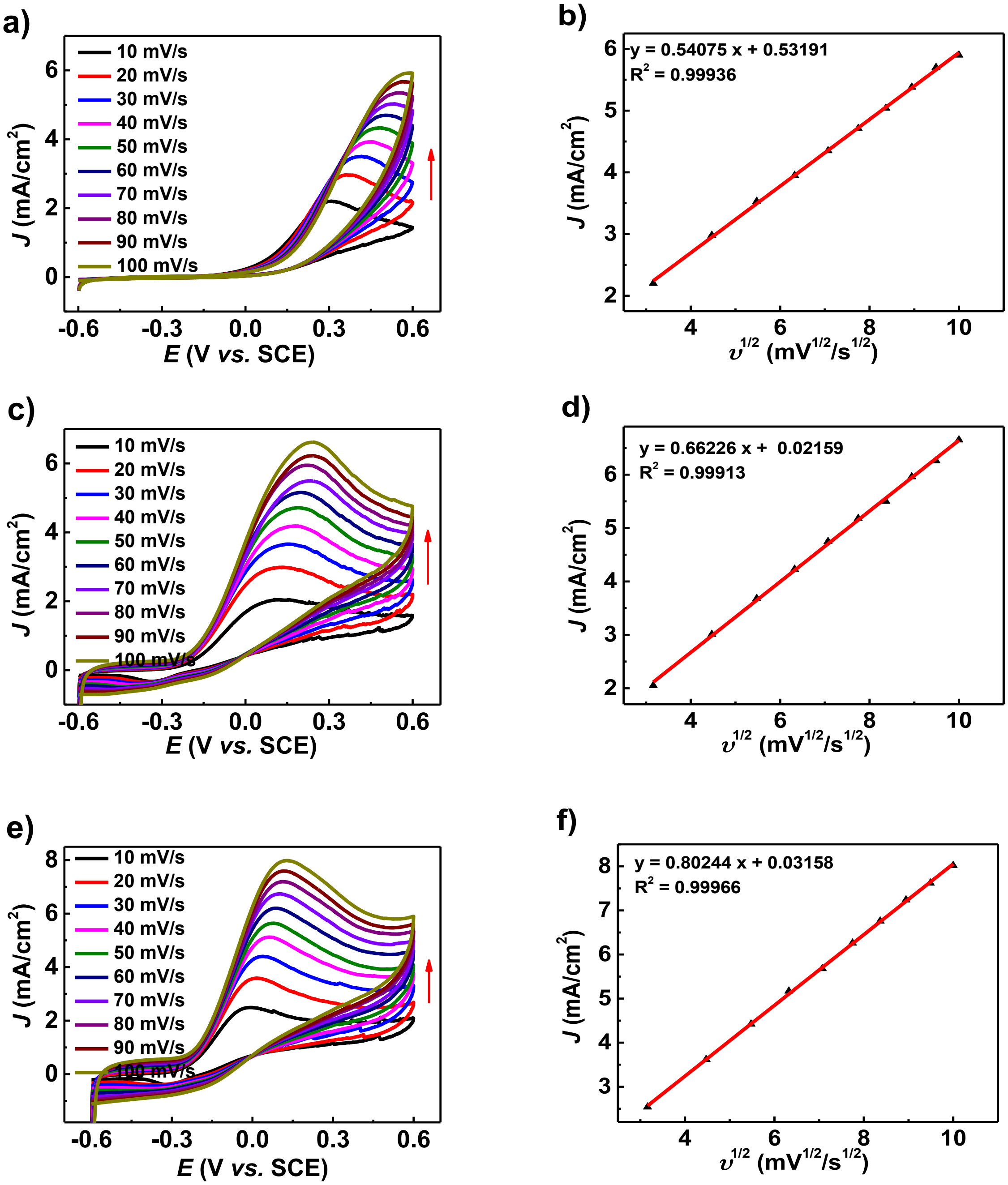
a)
10 mV/s
20 mV/s
30 mV/s
40 mV/s
50 mV/s
60 mV/s
70 mV/s
80 mV/s
90 mV/s
100 mV/s
J (mA/cm^2)
E (V vs. SCE)
-0.6
-0.3
0.0
0.3
0.6
0
2
4
6
b)
y = 0.54075 x + 0.53191
R^2 = 0.99936
J (mA/cm^2)
$\upsilon^{1/2}$ (mV$^{1/2}$/s$^{1/2}$)
4
6
8
10
2
3
4
5
6
c)
10 mV/s
20 mV/s
30 mV/s
40 mV/s
50 mV/s
60 mV/s
70 mV/s
80 mV/s
90 mV/s
100 mV/s
J (mA/cm^2)
E (V vs. SCE)
-0.6
-0.3
0.0
0.3
0.6
0
2
4
6
d)
y = 0.66226 x + 0.02159
R^2 = 0.99913
J (mA/cm^2)
$\upsilon^{1/2}$ (mV$^{1/2}$/s$^{1/2}$)
4
6
8
10
2
3
4
5
6
e)
10 mV/s
20 mV/s
30 mV/s
40 mV/s
50 mV/s
60 mV/s
70 mV/s
80 mV/s
90 mV/s
100 mV/s
J (mA/cm^2)
E (V vs. SCE)
-0.6
-0.3
0.0
0.3
0.6
0
2
4
6
8
f)
y = 0.80244 x + 0.03158
R^2 = 0.99966
J (mA/cm^2)
$\upsilon^{1/2}$ (mV$^{1/2}$/s$^{1/2}$)
4
6
8
10
3
4
5
6
7
8

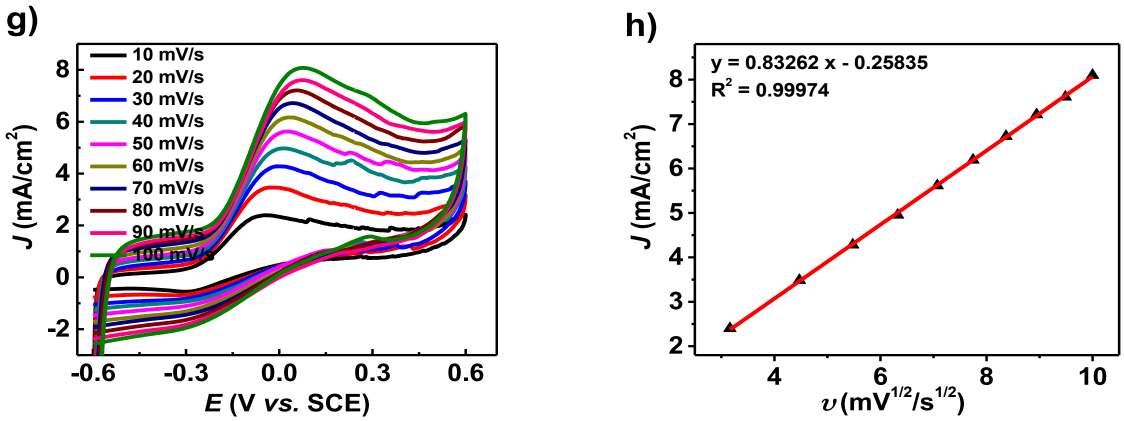

Figure S11. CVs for electrochemical oxidation of hydrazine (50 mM) at different scan rates, ranging from 10 mV/s to 100 mV/s, at pH at pH 7.4 in 0.1 M PBS over the series of RMDC-800-*x* materials (left panels) and the corresponding plot for peak current density versus square of scan rate plots (right panels). The CVs include: (a) RDC-800-0, (c) RDMC-800-0.5, (e) RDMC-800-1 and (g) RDMC-800-2. The corresponding plots of current density versus scan rate are for: (b) RDC-800-0, (d) RDMC-800-0.5, (f) RDMC-800-1 and (h) RDMC-800-2.

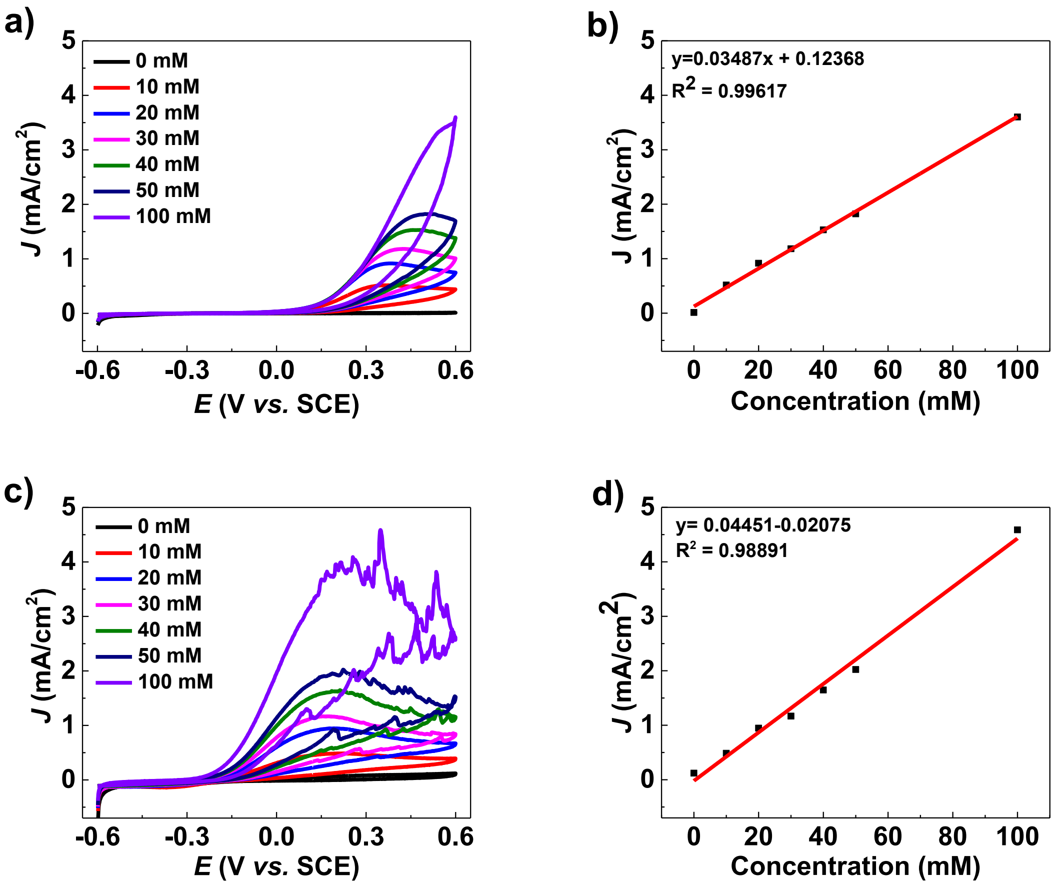

Figure S12. (a-d) CVs for electrochemical HOR for various concentrations of hydrazine over two control materials (left panels) and their corresponding peaks current density versus hydrazine concentration graphs (right panels). The results are displayed for sample RDMC-HTC-1 (a,b) and RDMC-800-Py-1 (c,d).

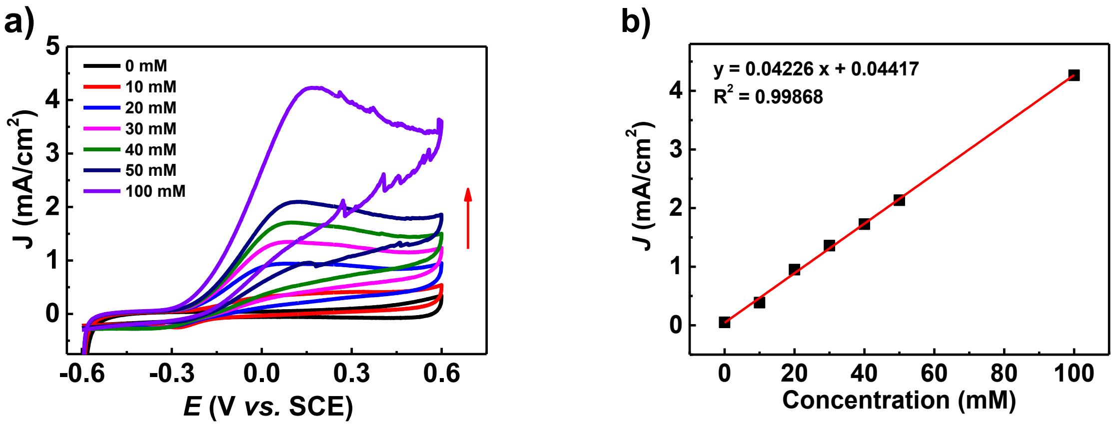

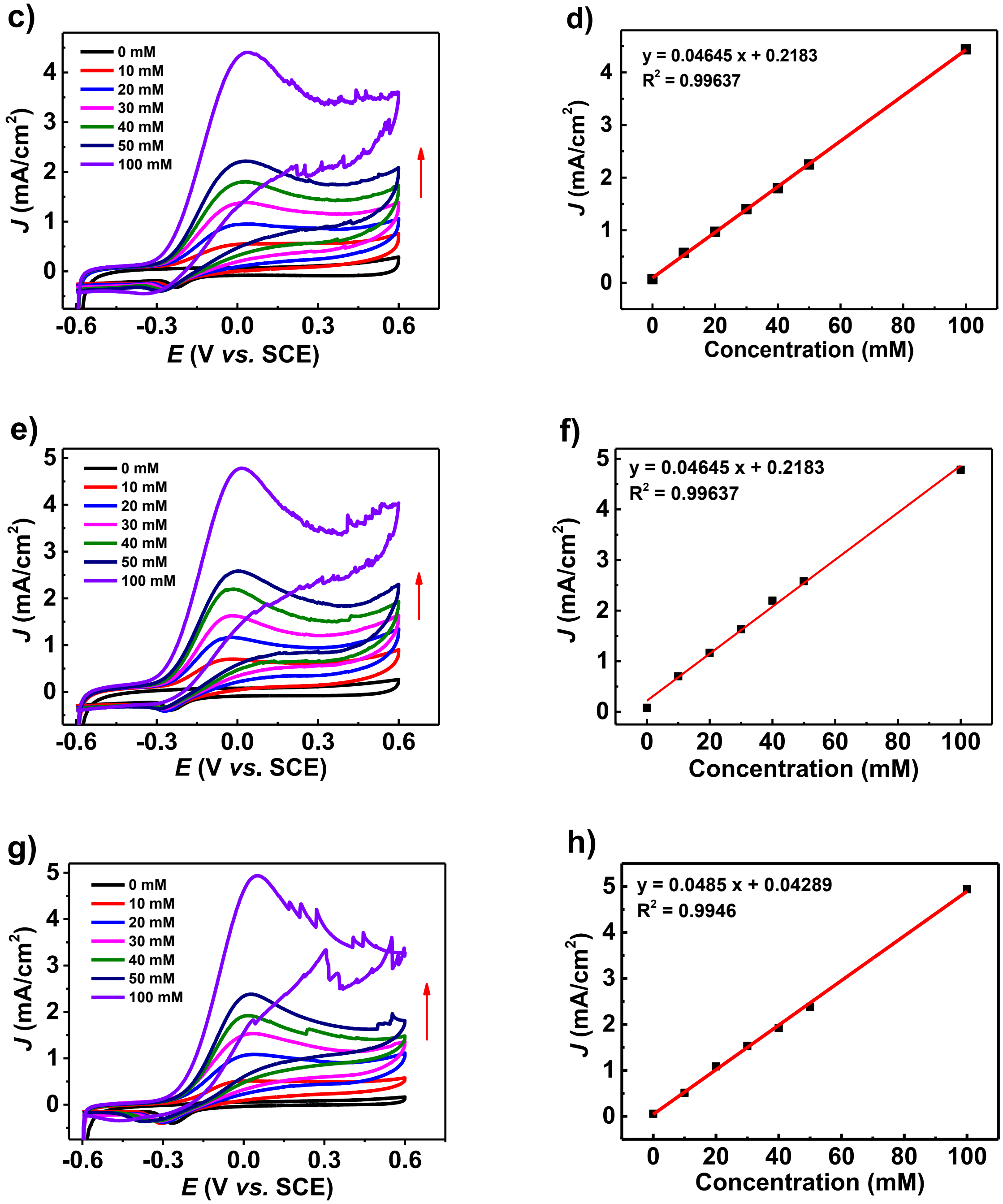

Figure S13. CVs of HOR obtained for various hydrazine concentrations at a scan rate of 10 mV/s at pH 7.4 in 0.1 M PBS over the series of RDMC-*T*-1 materials (left panels) and their corresponding graph of peak current density versus hydrazine concentration (right panels). The CVs are for: (a) RDMC-600-1, (c) RDMC-700-1, (e) RDMC-800-1, and (g) RDMC-900-1. The corresponding plots of current density versus concentration are shown for: (b) RDMC-600-1, (d) RDMC-700-1, (f) RDMC-800-1, and (h) RDMC-900-1.

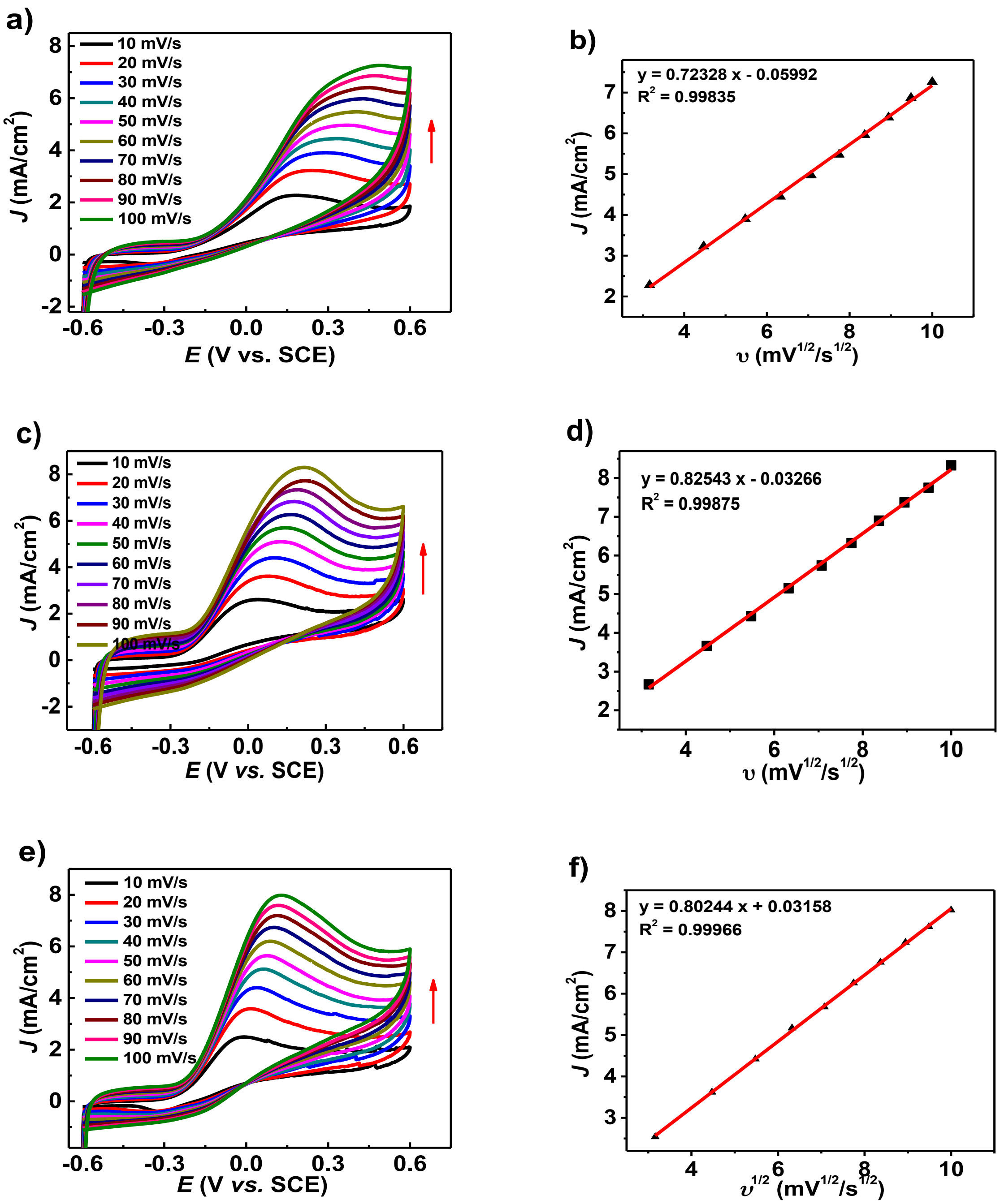
a)
10 mV/s
20 mV/s
30 mV/s
40 mV/s
50 mV/s
60 mV/s
70 mV/s
80 mV/s
90 mV/s
100 mV/s
J (mA/cm^2)
E (V vs. SCE)
-0.6
-0.3
0.0
0.3
0.6
-2
0
2
4
6
8
b)
y = 0.72328 x - 0.05992
R^2 = 0.99835
J (mA/cm^2)
υ (mV$^{1/2}$/s$^{1/2}$)
c)
10 mV/s
20 mV/s
30 mV/s
40 mV/s
50 mV/s
60 mV/s
70 mV/s
80 mV/s
90 mV/s
100 mV/s
J (mA/cm^2)
E (V vs. SCE)
d)
y = 0.82543 x - 0.03266
R^2 = 0.99875
J (mA/cm^2)
υ (mV$^{1/2}$/s$^{1/2}$)
e)
10 mV/s
20 mV/s
30 mV/s
40 mV/s
50 mV/s
60 mV/s
70 mV/s
80 mV/s
90 mV/s
100 mV/s
J (mA/cm^2)
E (V vs. SCE)
f)
y = 0.80244 x + 0.03158
R^2 = 0.99966
J (mA/cm^2)
υ$^{1/2}$ (mV$^{1/2}$/s$^{1/2}$)
4
6
8
10

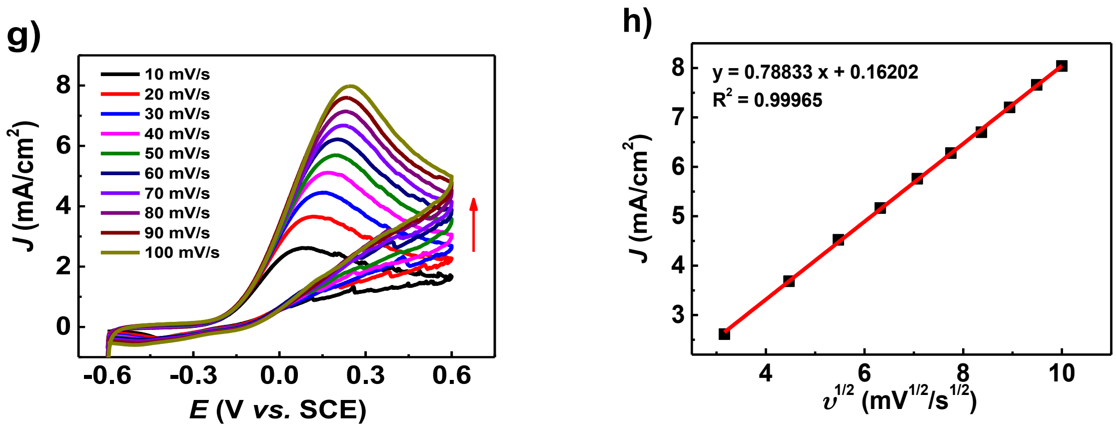

Figure S14. CVs of HOR for 50 mM hydrazine at different scan rates, ranging from 10 mV/s to 100 mV/s, at pH 7.4 in 0.1 M PBS over the series of RDMC-*T*-1 materials (left panels) and their corresponding peak current density versus square of scan rate plots (right panels). The CVs are for: (a) RDMC-600-1, (c) RDMC-700-1, (e) RDMC-800-1, and (g) RDMC-900-1. The corresponding plots of current density versus scan rate are for: (b) RDMC-600-1, (d) RDMC-700-1, (f) RDMC-800-1, and (h) RDMC-900-1.

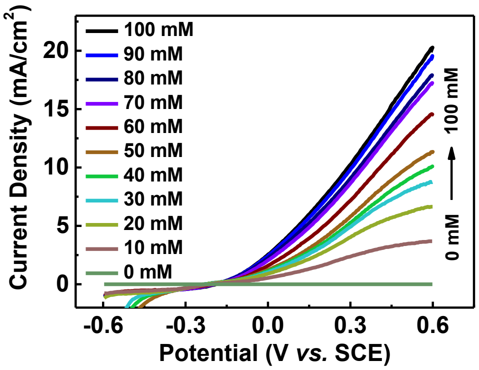

Figure S15. Polarization curves of hydrazine oxidation reaction (HOR) over RDMC-800-1. The measurement was performed at rotation speed of 900 rpm and at a scan rate 10 mV/s with different hydrazine concentrations in 0.1 M PBS solution.

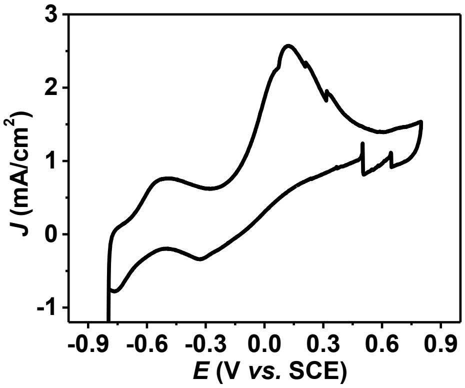

Figure S16. CVs of HOR obtained for 10 mM of hydrazine at 10 mV/s scan rate at pH 7.4 in 0.1 M PBS over Pt/C (20 wt. %) electrocatalyst.

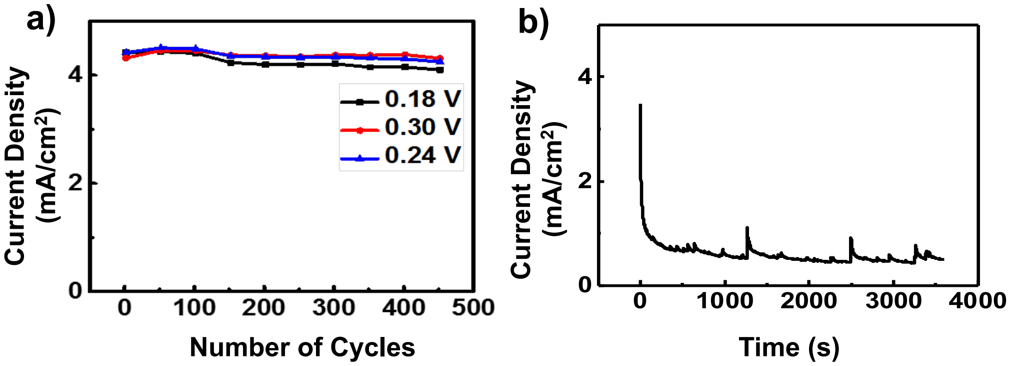

Figure S17. Stability test of RDMC-800-1 in 50 mM hydrazine, 0.1 M PBS at pH 7.4 during electrocatalysis of HOR over several cycles. a) Peak curent density of hydrazine electro-oxiation as function of number of electrocatalytic cycles and b) chronoamperometric curve at working potential of 1 mV (vs. SCE).

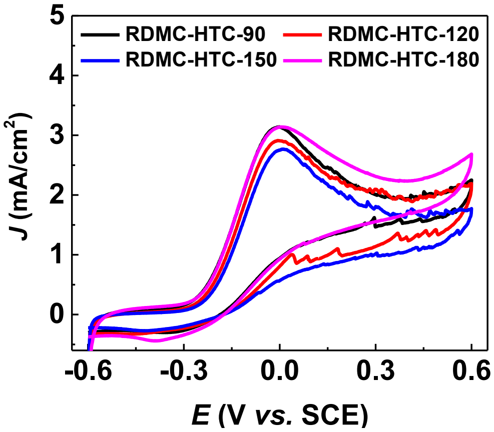

Figure S18. CVs of 50 mM hydrazine during electrochemical oxidation at pH 7.4 in 0.1 M PBS with scan rate of 10 mV/s over the different RDMC-HTC (control) materials, synthesized by varying the HTC temperature.

Table S3. Comparison of the structures and the electrocatalytic activity of RDMC-800-1 for HOR with respect to other notable, recently reported carbon electrocatalysts for the same reaction.

Sample	**Onset/Peak Potential (*vs.* SCE)**[a]	**BET Surface Area (m^2/g)**[b]	**BJH Average Pore Size (nm)**[b]	**Atomic % of N**[c]	**Ref.**
Carbon nanoneedle	0.15 / 0.7 V	-	-	9	[S1]
PPY-NOMPC-900	-0.36 / -0.06 V	400	3.7	3.29	[S2]
YCWC[d]	-0.38 / 0.04 V [e]	912	2.6	-	[S3]
PCDF-900	-0.3 / 0.1 V	493	4.3	0.4	[S4]
RDMC-800-1	**-0.34 / -0.002 V**	**366**	**12**	**0.7**	**This work**

[a] Obtained from CV of 50 mM hydrazine at pH 7.4 in 0.1 M PBS. [b] Obtained from N_2 adsorption/desorption isotherms. [c] Obtained with XPS. [d] YCWC also have Fe species inside, and its excellent electrocatalytic activity of this material is believed to be partly due to the metal species in it. [e] Obtained from CV of 64 mM hydrazine at pH 7.4 in 0.1 M PBS.

Table S4. Selected recent literature results of electrocatalytic activities of different nanomaterials for HOR compared with our results.

Electrode	Medium	Sweep Rate	Conc. [N_2H_4]	Onset / Peak Potential (*vs.* SCE)	Ref.
Pd/C	0.05 M H_2SO_4	20 mV/s	10 mM	-0.05/0.1 V	[S5]
Au/TiO_2-NTs/Ti	0.1 M pH 7.0 PBS	100 mV/s	0.85 mM	-0.05/0.25 V	[S6]
Au NP/GNP/GCE	0.1 M pH 6.0 PBS	100 mV/s	0.1 mM	-0.15/0.05 V	[S7]
CeO_2-RGO	3 M KOH	50 mV/s	22 mM	0.1/0.5 V	[S8]
Nanoporous gold	0.1 M pH 8.5 PBS	20 mV/s	10 mM	-0.3/0.0 V	[S9]
TiO_2-Pt NFs/GCE	0.1 M pH 7.0 PBS	100 mV/s	4 mM	0/0.6 V	[S10]
CM-MWCNT-GCE	0.5 M pH 8.0 PBS	25 mV/s	0.4 mM	0.05/0.2 V	[S11]
Pd/MWCNTs@Pd	0.1 M K_2SO_4	50 mV/s	5 mM	0/0.3 V	[S12]
Cu-GP	0.1 M KOH	100 mV/s	10 mM	-0.1/0.3 V	[S13]
Pt/TiO_2-NTs	0.1 M K_2SO_4	50 mV/s.	10 mM	0/0.25 V	[S14]
Au-NPs/PAni/Ti	0.5 M H_2SO_4	100 mV/s	2 mM	0.4/0.7 V	[S15]
RDMC-800-1	**0.1 M pH 7.0 PBS**	**10 mV/s**	**10 mM**	**-0.34/-0.002 V**	**This work**

References for SI Section

(S1) R. Silva, J. Al-Sharab, T. Asefa, *Angew. Chem. In. Ed.* 2012, **51**, 7171-7175.

(S2) Y. Meng, X. Zou, X. Huang, A. Goswami, Z. Liu, T. Asefa, *Adv. Mater.* 2014, **26**, 6510-6516.

(S3) X. Huang, X. Zou, Y. Meng, E. Mikmeková, H. Chen, D. Voiry, A. Goswami, M. Chhowalla, T. Asefa, *ACS Appl. Mater. Interfaces* 2015, **7**, 1978-1986.

(S4) A. C. Martins, X. Huang, A. Goswami, K. Koh, Y. Meng, V. C. Almeida, T. Asefa, *Carbon* 2016, **102**, 97-105.

(S5) Y. Liang, Y. Zhou, J. Ma, J. Zhao, Y. Chen, Y. Tang, T. Lu, *Appl. Catal. B* 2011, **103**, 388-396.

(S6) M. Hosseini, M. M. Momeni, M. Faraji, *J. Mol. Catal. A: Chem.* 2011, **335,** 199-204.

(S7) Q. Wana, Y. Liua, Z. Wang, W. Wei, B. Li, J. Zou, N. Yang, *Electrochem. Commun.* 2013, **29**, 29-32.

(S8) M. Srivastavaa, A. K. Dasa, P. Khanraa, M. E. Uddina, N. H. Kim, J. H. Lee, *J. Mater. Chem. A* 2013, **1**, 9792-9801.

(S9) X. Yan, F. Meng, S. Cui, J. Liu, J. Gu, Z. Zou, *J. Electroanal. Chem.* 2011, **661**, 44-48.

(S10) Y. Ding, Y. Wang, L. Zhang, H. Zhang, C. M. Li, Y. Lei, *Nanoscale* 2011, **3**, 1149-1157.

(S11) L.Zheng, J.-F. Song, *Senso. Actuat. B: Chem.* 2009, **135**, 650-655.

(S12) W. Ye, H. Hu, H. Zhang, F. Zhou, W. Liu, *Appl. Surf. Sci.* 2010, **256**, 6723-6728.

(S13) H. Gao, Y. Wang, F. Xiao, C. B. Ching, H. Duan, *J. Phys. Chem. C* 2012**, 116***,* 7719-7727.

(S14) B. Dong, B.-L. He, Y.-M. Chai, C.-G. Liu, *Mater. Chem. Phys.* 2010, **120**, 404-408.

(S15) M. G. Hosseini, M. M. Momen, S. Zeynali, *Surf. Eng.* 2013, **29**, 65-69.